Fe–N–C single-atom catalysts with an axial structure prepared by a new design and synthesis method for ORR

*Fan Liu, Ning Yan, Guangqi Zhu, Zigeng Liu, Shenqian Ma, Guolei Xiang, Songrui Wang, Xingjiang Liu, Wei Wang**

F.Liu, N. Yan, G.Q. Zhu, X. Meng, Prof. W. Wang

School of Chemical Engineering and Technology, Tianjin University, Tianjin, China

E-mail: wangweipaper@tju.edu.cn

Z.G. Liu

Max Planck Institute for the Advancement of Science, Germany

S.Q. Ma, Prof. G.L. Xiang

State Key Laboratory of Chemical Resource Engineering, College of Chemistry, Beijing University of Chemical Technology, Beijing 100029, China

S.R. Wang, X.J. Liu

The 18th Research Institute of China Electronics Technology Group Corporation, China

Fan Liu and Ning Yan are the co-first authors.

* are the Corresponding authors

Keywords: monatomic catalyst, Fe-N_5 active site, Fe-N_4 active site, synthesize, ORR activity

Fe–N–C single-atom catalysts usually exhibit poor ORR activity due to their unsatisfactory O2 adsorption and activation. Here, a new design idea and tailored self-assembly synthesis method are reported to improve their ORR performance. DFT calculations have been widely used to design the catalysts for ORR in fuel cell. Our studies on DFT calculations indicate that the ORR electrocatalytic activity of Fe-N_5 active site embedded in carbon six-member rings is superior to that of Fe-N_4 active site. In order to experimentally demonstrate the difference, Fe-N_5-C/G monatomic catalysts with Fe-N_5 active site were successfully synthesized on the surface of monolayer graphene. XANES, SEM, HRTEM, XRD, Raman and XPS analyses indicate that

synthesized Fe-N_5-C/G catalyst possessed nanofibre morphology and a curved layer-like crystal structure. For comparison, FePc powders were used as FePc(Fe-N_4) catalyst for its molecular structure involving a Fe-N_4 active site embedded in carbon six-member rings. The current density of synthesized Fe-N_5-C/G catalyst at potential 0.88V vs RHE is 1.65 mA/cm^2 , which is much higher than that of FePc(Fe-N_4) catalyst (1.04 mA/cm^2), and even higher than that of commercial Pt/C catalyst (1.54 mA/cm^2). The results are consistent very well with the DFT calculations, verifying the dependability and accuracy of DFT calculation. This work reports a new synthetic idea to obtain better performance and proposes a formation mechanism to explain the process of the synthesis method.

1.Introduction

Oxygen reduction reaction (ORR) is generally regarded as a pivotal cornerstone and a limiting step in several sustainable energy storage and conversion devices.[1-4] Tremendous efforts have been devoted to developing catalysts to overcome the sluggish reaction kinetics.[5-8] To date, Pt group materials perform the best performance in case of ORR catalysts.[9] However, their practical applications are limited by a few of fatal defects including sensitivity to poisoning, scarcity and prohibitive cost. To overcome these barriers and implement large-scale application, researches on non-noble metal electrocatalysts have attracted wide attention.[10-12]

In recent years, a wide range of low-cost materials, including nanostructured carbons,[13-14] non-noble transition metal oxides,[15-16] carbides/nitrides and their composites,[17-19] and non-precious transition metals (e.g., Fe or Co) and nitrogen (N) co-doped carbon (denoted as M-N-C) have been shown to possess moderate activity towards oxygen electrocatalysis. Especially, the Fe-N-C represents the state-of-the-art catalysts towards ORR, which has exhibited catalytic activity approaching to that of commercial Pt/C catalysts in alkali.[20-24] Fe-N-C catalysts are emerging as a promising candidate for the ORR catalyst relying on the electrochemical stability

of carbon support,[25] good electrical conductivity, stable chemical bonds and efficient active sites.[26-30] Wan and coworkers developed a cascade anchoring strategy for mass production of single-atomic metal-nitrogen catalysts with a high loading of metal up to 12.1 wt.%. A simple ionothermal method was also developed to fabricate highly reactive and stable single-atom ORR catalysts, atomically dispersed Fe-Nx species on porous porphyrinic triazine-based frameworks with high Fe loading up to 8.3 wt.%.[17] Besides improving the intrinsic activity by engineering single-atomic Fe-N_x moiety, creating a high concentration of defects as active sites in carbon-based materials will further elevate the ORR electrochemical process.[18-20] Yao's group reported that carbon defects could introduce unsaturated carbon atoms with dangling bonds and reshape the local electronic structure, thus improving the electrocatalytic activity.[21] Liu et al suggested that the defect sites with dangling bonds would react with oxygen after exposure to air, resulting in oxygen functionalization and enhancement of catalytic activities.[22]

DFT calculations have been widely used in the design of ORR catalysts.[31-32] The accuracy of DFT calculations is being paid close attention to. Our researches on the active site Fe-N_x (x=1-5) coordination structures embedded in carbon six-member rings through DFT calculations indicated that the ORR electrocatalytic activity of active sites Fe-N_5 is superior to that of active sites Fe-N_4, and even better than that of Pt(111).[39] The results are very useful for the design of ORR electrocatalysts and needed to be proved in practice. Aiming at this, two kinds of catalysts with the active sites embedded in carbon six-member rings, one is FePc(Fe-N_4) catalyst with Fe-N_4 active site and the other is synthesized Fe-N_5-C/G catalyst with Fe-N_5 active site, are chosen as the objects to study. Fe-N_5-C/G catalyst was synthesized through an organic tailoring-self-assembling-crystallizing vapor deposition (TSCVD) technology developed in our lab. EXAFS, SEM, HRTEM, XRD, XPS, Raman analyses were conducted to characterize the structure of synthesized Fe-N_5-C/G catalyst. The electrochemical analyses indicated that an efficient four-electron transfer process proceeded on Fe-N_5-C/G catalyst while

a two-electron transfer process occur on FePc(Fe-N_4) catalyst during ORR process. The electrocatalytic activity of Fe-N_5-C/G catalyst was notably superior to that of FePc(Fe-N_4) catalyst and even better than that of commercial Pt/C catalyst. The experimental results are consistent very well with that obtained through DFT calculations, proving the dependability and accuracy of DFT calculation.

2.Results and Discussion

2.1. Synthesis of the catalyst with Fe-N_5 active site

The synthetic strategy for Fe-N_5-C/G catalyst involved three steps. The first step was to synthesize graphene monolayer on Cu foil (noted as G/Cu). The second step was to synthesize Fe-N_5-C catalyst on the surface of the graphene monolayer in G/Cu (noted as Fe-N_5-C/G/Cu). The third step was to remove the Cu layer in Fe-N_5-C/G/Cu and get Fe-N_5-C/G catalyst.

The synthesizing process for the graphene monolayer is schematically illustrated as follow: Firstly, an electrodeposition method was used to deposit Cu foils on the surface of a stainless steel sheet. Then, the deposited Cu foils was peeled off from the sheet. The Cu foil was used as the substrate and put into a tube furnace to synthesize graphene monolayer through a CVD process,[33] in which a mixture gas with 12 sccm of CH_4 gas and 48 sccm of H_2 gas flew through the tube furnace and the temperature was controlled at 1000°C for 60 min.

The synthesizing process for Fe-N_5-C/G catalyst is schematically described as follow: a quartz boat loaded with FePc powders as the precursor and a G/Cu sheet were put into a tube furnace in separate positions at different temperatures. Precursor FePc powders was heated at 450°C for 30min under argon gas atmosphere and sublimated into the space companied with the removal of the H atoms in FePc molecules. Then flowing argon gas was let into the tube furnace for 120 minutes to drive the molecules to the position placed with G/Cu sheet at 70°C to form the catalyst (noted as Fe-N_5-C/G/Cu).

The copper layer in Fe-N_5-C/G/Cu was removed by floating the synthesized Fe-N_5-C/G/Cu on the surface of 0.1 M $FeCl_3$ solution for more than 12h. Then the remained Fe-N_5-C/G films were washed with deionized water three times and dried in an oven at 60°C to get Fe-N_5-C/G catalyst.

2.2. Materials characterization

The scanning electron microscopy (SEM) observations were performed with a field-emission Hitachi s-4800 and SEM/energy-dispersive X-ray (EDX) spectroscopy mapping was undertaken on an Ametek EDAX at an acceleration voltage of 15 kV. Transmission electron microscopy (TEM) and high-resolution transmission electron microscopy (HRTEM) images were obtained on JEM-2100F operated at acceleration voltages of 80 kV and 200 kV, respectively. X-ray diffraction (XRD) was performed on a Bruker D8-Focus system with Cu Kα radiation (λ=1.5419Å). The X-ray absorption data at the Fe K-edge of the samples were recorded at beamline 1W1B in Beijing Synchrotron Radiation Facility (BSRF). The station was operated with a Si (111) double crystal monochromator in transmission mode and fluorescence mode, respectively. During the measurement, the synchrotron was operated at 3.5 GeV and the current was between 150-210 mA. The data for each sample were calibrated with standard Fe metal foil. Data processing was performed using program Athena. Extended X-ray absorption fine structure (EXAFS) spectra were fitted using program Artemis. X-ray photoelectron spectroscopy (XPS) was performed using a PHI5000 Versa Probe. The energy calibration of the spectrometer was performed using C 1s peak at 284.5 eV.

Fourier Transform Infrared Spectroscopy (FTIR) was conducted on a Bruker ALPHA system with an ATR technique attachment. Raman Spectrum was performed on a RENISHAW in via reflex with an incident ray source (λ=532 nm). Thermogravimetric analysis (TGA) was

performed on a TA Q500 thermal gravimetric analyzer in a N_2 atmosphere at a heating rate of 5 °C min^{-1}.

2.3. Electrochemical measurements

Electrochemical measurements were performed with a CHI660D electrochemical workstation in a typical three-electrode system. The catalyst supported on a glassy carbon electrode (GCE) with a diameter of 5 mm was served as the working electrode, whereas ruthenium-titanium mesh and Hg/HgO (1 M KOH) electrode were used as the counter and reference electrodes, respectively. All the potentials given are relative to reversible hydrogen electrode (RHE): E(vs RHE) = E(vs Hg/HgO) + 0.098 + 0.059pH. All the electrochemical measurements were carried out using a rotating disk electrode (RDE) device in an O_2- or N_2-saturated 0.1 M KOH solution at 25±1°C. Cyclic voltammetry (CV) in a potential range of 0.2 ~1.2 V was performed at a scan rate of 50 mV s^{-1}. The linear scan voltammetrys (LSV) were conducted at potential scan rates of 5 mV s^{-1}. Electrochemical impedance spectroscopy (EIS) was measured at potential 0.91V by applying an AC amplitude of 5 mV and frequency from 1 to 10^5 Hz. The durability tests were conducted by measuring the current vs. time (i-t) chronoamperometric response at potential 0.925V for 40000s.

Related measurements were also conducted for FePc powders (20wt%, Alfa Aesar), commercial Pt/C catalyst (Pt 20wt%, Alfa Aesar) and synthesized graphene monolayer on the Cu foil (G/Cu). The details for the preparation of the electrode were mentioned in earlier report.[34]

The electron transfer number (n) involved in the ORR was calculated according to Koutecky-Levich (K-L) plots.[35-38]

$$\frac{1}{J} = \frac{1}{J_L} + \frac{1}{J_K} = \frac{1}{B\omega^{1/2}} + \frac{1}{J_K} \qquad (1)$$

Where J is the measured current density, J_K the diffusion-limited current densit, ω the electrode rotation rate.

$$B = 0.2nFC_0(D_0)^{2/3}\nu^{-1/6} \quad (2)$$

Where F is Faraday constant (96485 C mol^{-1}), C_0 the bulk concentration of O_2 (1.2×10^{-3} mol L^{-1} for 0.1 M KOH solution), D_0 the diffusion coefficient of O_2 (1.9×10^{-5} cm^2 s^{-1} for 0.1 M KOH solution), ν the kinetic viscosity of the electrolyte (0.01 cm^2 s^{-1} for 0.1 M KOH aqueous solution), k the electron transfer rate constant.

2.4. Design of the active sites and synthetic route

Fig. 1a) and b) show the structural models of the catalysts with different coordination structure Fe-N_x (x=1-5) active sites embedded in carbon six-member rings and their ORR overpotentials calculated by DFT in our previous work.[39] The desired atomic model should have the following characteristics:

1. In the double vacancy (DV), as the number of doped N atoms increases, the formation energy Ef becomes increasingly negative, resulting in Fe-4N defects being the most stable in the Fe-N-C catalyst.

2. The overpotential of the catalyst with double vacancy structure decreases with the incorporation of N atoms. It can be concluded that in the double-vacancy structure, the incorporation of an appropriate number of N atoms and different doping configurations can improve the ORR catalytic performance of the Fe-N coordination structure.

3.In the double-vacancy structure, the bond length of the Fe-O bond gradually increases as the number of N atoms increases. The interaction between Fe atoms and O atoms gradually weakens, weakening the strong binding force between oxygen-containing compounds and their surface sites will increase ORR activity.

Based on the above three points (shown in Fig S1), a molecule with Fe-N_5 active site was modeled. All the ORR overpotentials for different active sites locate in a straight line. The ORR overpotentials of the catalyst with five-coordination Fe-N_5 active site (0.33 V) is the lowest, which is much lower than that with four-coordination Fe-N_4 active site (0.46 V) and even a little lower than Pt (111). The results reveal that the catalyst with five-coordination Fe-N_5 active site is more effective to catalyze ORR compared with the catalyst with four-coordination Fe-N_4 active site. Considering the structure of iron phthalocyanine molecule (FePc) (Fig. 1c), a four-coordination Fe-N_4 active site is located in the center and four carbon six-member rings surround it, which is very close to the designed structural model of the catalyst with four-coordination Fe-N_4 active site except the H atoms connected with the surrounding carbon six-member rings. So, FePc powders was chosen as the catalyst with four-coordination Fe-N_4 active site and noted as FePc(Fe-N_4) catalyst.

Considering the TG curve of FePc powders as shown in Fig.1d), a dehydrogenation process accompanied with a sublimation process occurs in a temperature range of 360~500°C. After getting rid of the H atoms in FePc molecules, a kind of unstable fragments generates (Fig. 1c). The length dimension of the generated unstable fragments is 1.02 nm. We speculate that a new catalyst with Fe-N_5 active site can be synthesized through the crystallization of the unstable fragments. Based on the consideration, FePc powders was chosen as the precursor to synthesize a new catalyst with Fe-N_5 active site.

A unique synthetic route was designed to synthesize the new catalyst in a tube furnace. Firstly, FePc powders were heated at 450°C. During the heating process, FePc molecules sublimated and the H atoms in FePc molecules were gotten rid of at the same time. The heating process at 450°C generated a lot of unstable fragments in the space. We called the process tailoring. Then the unstable fragments mutually self-assembled to form self-assembly units in

the space. We called the process self-assembling. Subsequently the self-assembly units were driven by flowing argon gas to another position placed with G/Cu foil at 70°C and crystallized on the surface of graphene monolayer to form the catalyst. We called the process crystallizing.

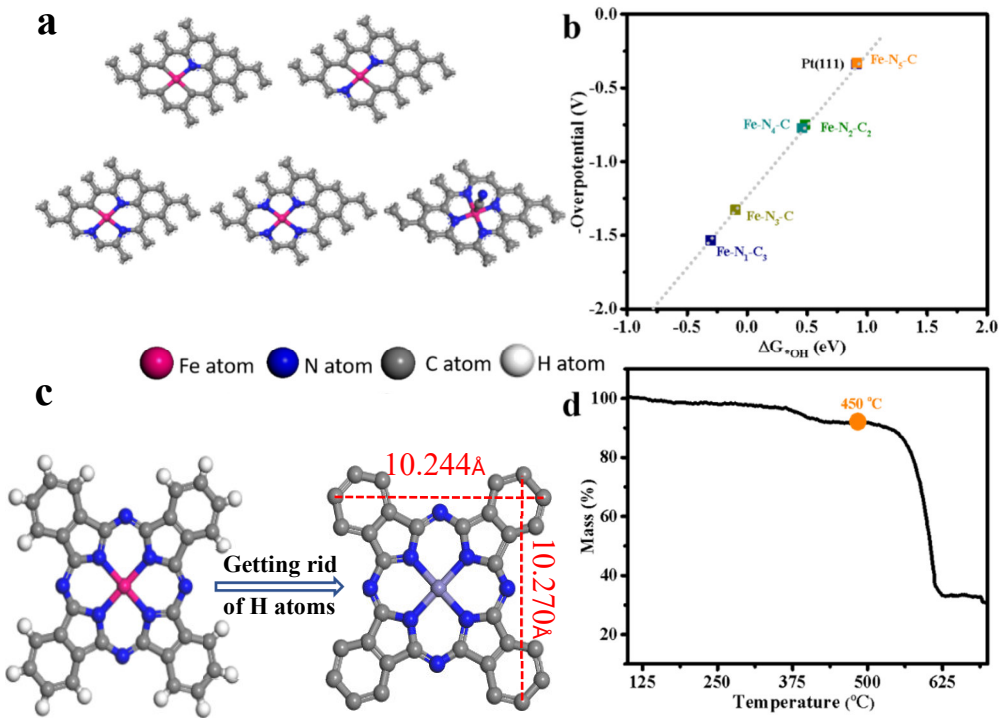

Figure 1. a) Optimized geometries of Fe-N_x（x=1-5）active site embedded in carbon six-member rings, b) Relations between the ORR overpotentials and $\Delta G^{*}OH$, c) Ball and stick model of FePc molecule and the fragment after getting rid of the H atoms, d) TGA curve of FePc powders.

2.5. Analyses on the coordination structure of synthesized Fe-N_5-C/G catalyst

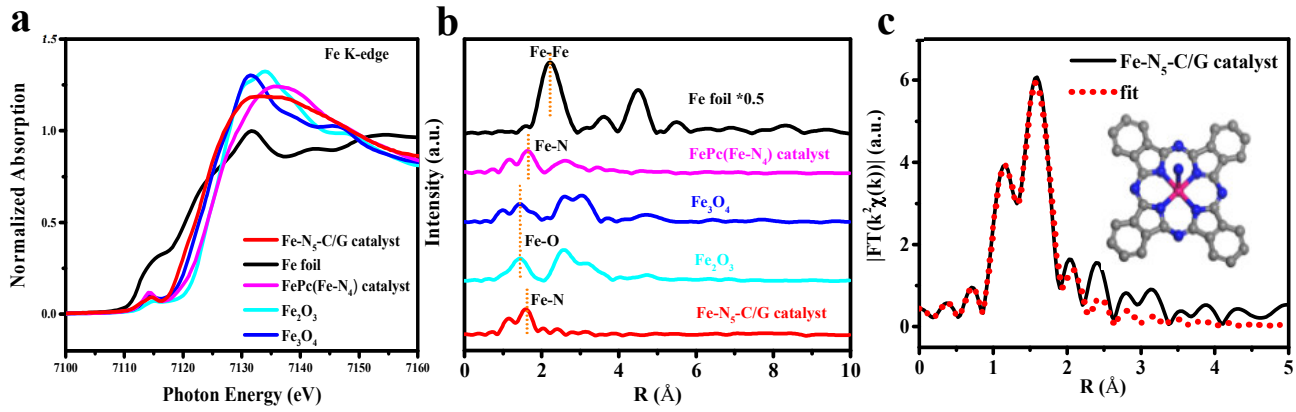

Figure 2. a) Normalized XANES spectra of Fe K-edge with different adsorption energy for Fe-N_5-C/G catalyst, FePc(Fe-N_4) catalyst, Fe foil, Fe_2O_3 and Fe_3O_4, respectively; b) FT-EXAFS spectra at Fe K-edge for Fe foil, Fe_2O_3, Fe_3O_4, FePc(Fe-N_4) catalyst and Fe-N_5-C/G catalyst, respectively; c) The corresponding EXAFS fitting curves for Fe-N_5-C/G catalyst. Inset: the structural model of the catalyst with five-coordination Fe-N_5 active site.

To explore the coordination structure of synthesized Fe-N_5-C/G catalyst , X-ray absorption near-edge structure (XANES) and extended X-ray absorption fine structure (EXAFS) were performed.[40] Fig. 2a) shows the normalized Fe K-edge XANES spectra of synthesized Fe-N_5-C/G catalyst and several reference materials as Fe foil, Fe_2O_3, Fe_3O_4 and FePc(Fe-N_4) catalyst. The XANES spectrum of Fe-N_5-C/G catalyst shows a near-edge absorption energy close to FePc(Fe-N_4) catalyst, implying the valence of element Fe is +2 in Fe-N_5-C/G catalyst. Fig. 2b) shows the Fourier transformations of the k_2-weighted EXAFS spectra (FT-EXAFS). It can be found that there is a single main peak at about 1.42Å for Fe-N_5-C/G catalyst, which can be attributed to Fe-N scattering paths. Fe-Fe peak at 2.2Å was not detected. The results prove the existence of Fe-N coordination in Fe-N_5-C/G catalyst. A least-square FT-EXAFS fitting based on the first strong peaks of Fe-N_5-C/G catalyst and FePc(Fe-N_4) catalyst was performed. Fig. 2c) shows the fitting curve of Fe-N_5-C/G catalyst, which matches well with the measured

spectrum. The fitting data are listed in table 1. Where, N represents the coordination number of Fe (II), R the mean length of the bond, σ^2 the Debye-Waller factor value. The coordination numbers of the Fe (II) are 5 and 4 for Fe-N_5-C/G catalyst and FePc(Fe-N_4) catalyst, corresponding to average bond lengths of 1.99 Å and 1.85 Å, respectively. Based on the analyses, the coordination structure of the Fe (II) in Fe-N_5-C/G catalyst can be considered as follows: a central Fe (II) is five-fold coordinated by five surrounding N atoms, in which four N atoms are located in the same plane and one N atom is located in the upper side of the plane. The five-coordination structure model is illustrated in Fig. 2c). The results above exhibit that a new catalyst with the designed five-coordination structure Fe-N_5 active site was successfully synthesized by the designed synthetic route.

Table 1 Fitting results of the FT-EXAFS spectra for Fe-N_5-C/G catalyst and FePc(Fe-N_4) catalyst

Sample	Path	N	R(Å)	$\sigma^2(10^{-3}Å^2)$
FePc(Fe-N_4) catalyst	Fe-N	4	1.85	0.0038372
Fe-N_5-C/G catalyst	Fe-N	5	1.99	0.0288832

2.6. Analyses on the structure and morphology

Fig. 3a) is the SEM images of FePc(Fe-N_4) catalyst, exhibiting a powder-like morphology. Fig. 2b)-c) are the SEM images of synthesized Fe-N_5-C/G catalyst. It can be found from Fig. 3b)-c) that Fe-N_5-C/G catalysts possess nanofibre morphology with smooth surface. The filiform catalysts interconnect with each other and their diameter is in the range of 10 nm-50 nm. The HR-TEM image (Fig. 3d) shows a layer structure with a interlayer spacing of 3.19 Å (inset). On closer inspection, there are great amounts of double-layer structural units joined together in a straight or curved way. The length of the double-layer structural units is in the range of 1nm-4nm, which is one to four times the length of the unstable fragments (1.02nm) generated

through getting rid of the H atoms in FePc molecules. Based on the analyses, it can be speculated that the filiform Fe-N_5-C/G catalyst are formed through the crystallization of a double-layer structural units. The double-layer structural units are composed of two unstable fragments generated through getting rid of the H atoms in FePc molecules.

The elemental mappings (Fig. 3f) indicate that elements C, N, and Fe homogeneously distribute throughout the whole filiform catalyst. Fig. 3e) shows the XRD pattern of Fe-N_5-C/G catalyst and FePc(Fe-N_4) catalyst. The XRD pattern of FePc(Fe-N_4) catalyst is consistent with the standard XRD card of α-FePc (PDF#20-1718), verifying that FePc(Fe-N_4) catalyst belongs to α-FePc. The remarkable difference in the peak positions of the XRD patterns between Fe-N_5-C/G catalyst and FePc(Fe-N_4) catalyst reveals that synthesized Fe-N_5-C/G catalyst possesses a new structure differing from FePc(Fe-N_4) catalyst, the precursor. The peak at 28° corresponds to a lattice spacing 3.19 Å, which is the same with the observed interlayer spacing in Fig. 3d). The results above indicate that synthesized Fe-N_5-C/G catalyst possesses nanofibre morphology and a curved layer-like crystal structure differing from FePc(Fe-N_4) catalyst.

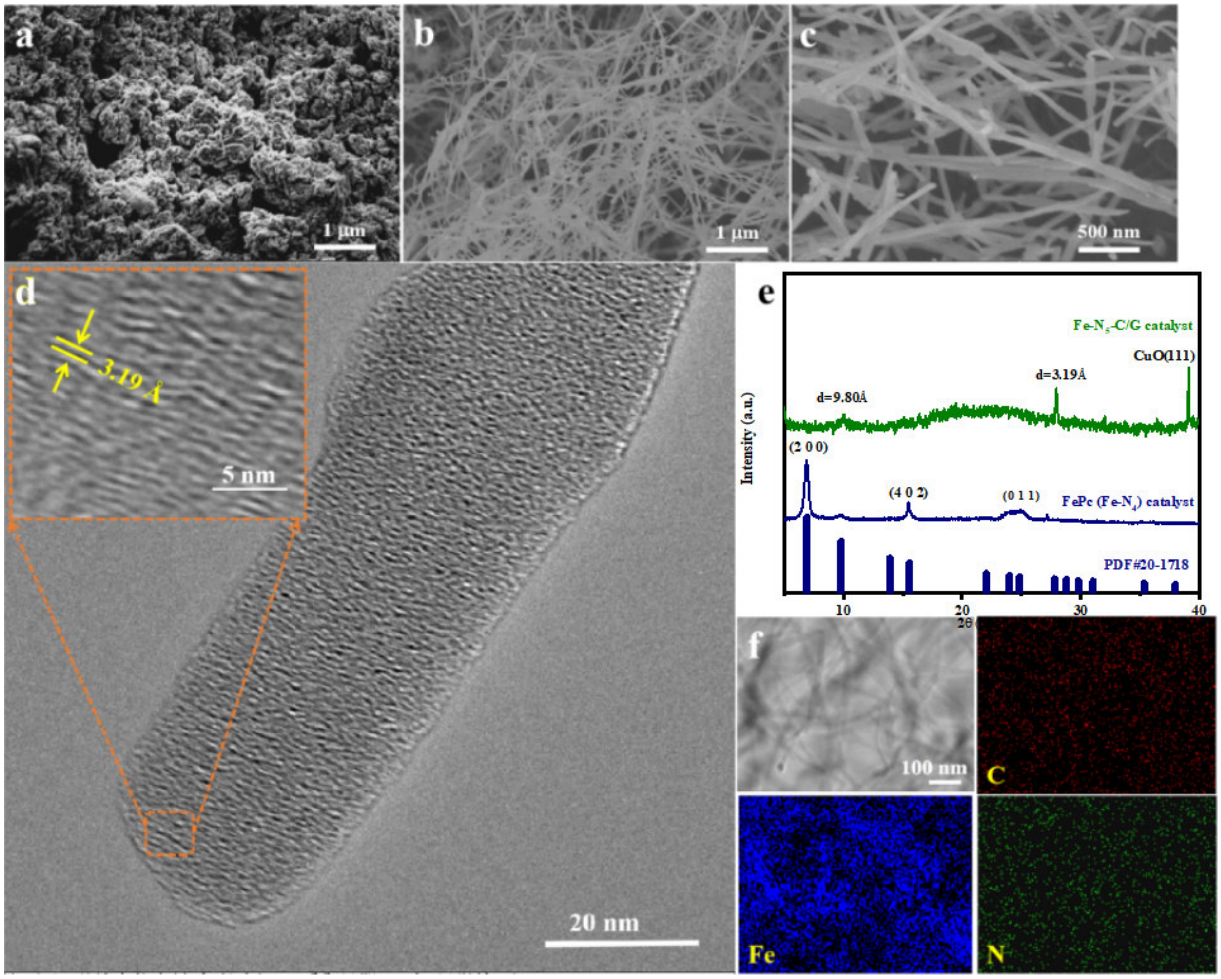

Figure 3. SEM images of a) FePc (Fe-N_4) catalyst and b)-c) synthesized Fe-N_5-C/G catalyst, d) HR-TEM images of Fe-N_5-C/G catalyst (the inset is the amplified view), e) XRD patterns of Fe-N_5-C/G catalyst and FePc (Fe-N_4) catalyst, f) Element mapping of C, Fe, and N for Fe-N_5-C/G catalyst, respectively.

2.7. Raman and XPS analyses

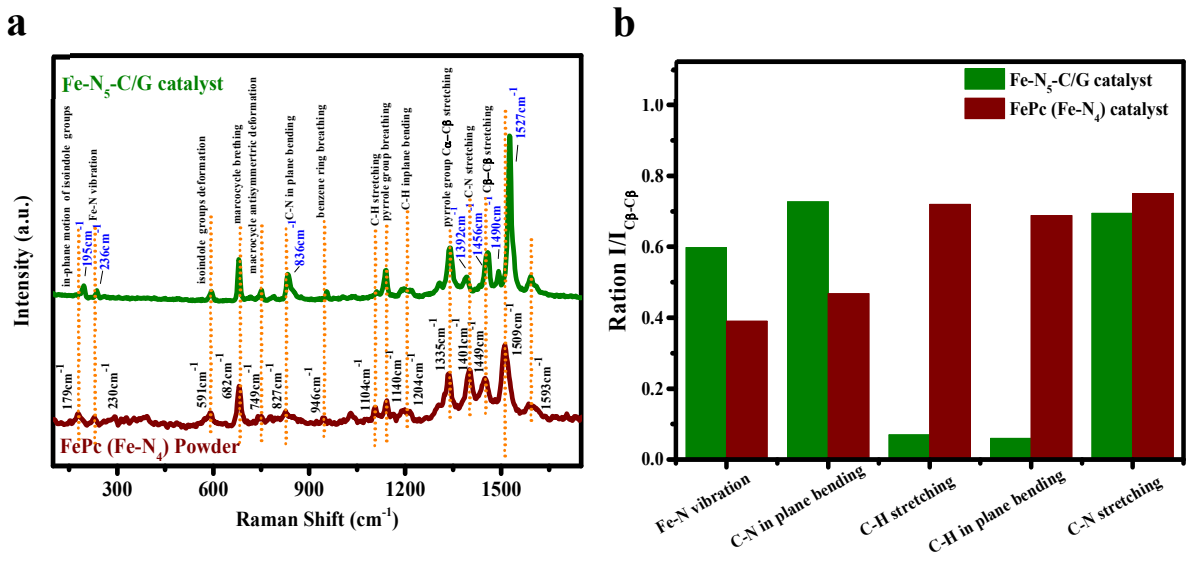

Figure 4. a) Raman spectrums of Fe-N_5-C/G catalyst and FePc (Fe-N_4) catalyst, b) Peak intensity ratio $I_m/I_{C\beta-C\beta}$ calculated by the data in figure a).

Fig. 4a) displays the Raman spectrums of FePc(Fe-N_4) catalyst and synthesized Fe-N_5-C/G catalyst. The peaks located at 1449 cm^{-1} and 1456 cm^{-1} are all caused by the vibration of C_β-C_β bonds in FePc(Fe-N_4) catalyst and Fe-N_5-C/G catalyst, respectively. C_β-C_β bonds in FePc(Fe-N_4) catalyst and Fe-N_5-C/G catalyst are stable during the synthetic process. To clearly understand the variation of the coordination structure, the peak intensity ratios I_m/ $I_{C\beta-C\beta}$ were calculated and shown in Fig.4b). Where, I_m represents the peak intensity of bond m in the Raman spectrums, m represents different kinds of bonds, $I_{C\beta-C\beta}$ represents the peak intensity of C_β-C_β bond in the Raman spectrums. The peaks at 179, 230, 682, 827 and 1401 cm^{-1} for FePc(Fe-N_4) catalyst, induced separately by the in-plane motion of the isoindole group, Fe-N stretching vibration, macrocycle breathing vibration and the two types of C-N stretching vibration,[41] also appear in synthesized Fe-N_5-C/G catalyst. The result above indicates that the macrocyclic structure in FePc(Fe-N_4) catalyst remains in synthesized Fe-N_5/G catalyst. For Fe-N_5-C/G catalyst, ratio I_{C-N} / $I_{C\beta-C\beta}$ for C-N bond in plane bending vibration (Fig.4b) gets much

higher compared with FePc(Fe-N_4) catalyst, and the same variation also appears for Fe-N vibration, implying that the numbers of C-N bond and Fe-N bond increase in Fe-N_5-C/G catalyst. Obvious peak shift from 230 cm^{-1} for FePc(Fe-N_4) catalyst to 236 cm^{-1} for Fe-N_5-C/G catalyst is observed for Fe-N stretching vibration. Moreover, the peak located at 1509 cm^{-1} for FePc(Fe-N_4) catalyst, which represents the bonds in-plane vibration between Fe and pyrrole-like N atoms, blue shifts to 1527 cm^{-1} for Fe-N_5-C/G catalyst. The shift indicates that the chemical surroundings of Fe(II) in Fe-N_5-C/G catalyst is different from that in FePc(Fe-N_4) catalyst. The ratio $I_{C\text{-}N}$ / $I_{C\beta\text{-}C\beta}$ of the peaks at 1104 and 1204 cm^{-1} for Fe-N_5-C/G catalyst, which correspond to the vibrations of C-H bond in FePc(Fe-N_4) catalyst, are very low compared with FePc(Fe-N_4) catalyst, indicating that C-H bonds no longer exist in Fe-N_5-C/G catalyst.

Based on the analyses above, it can be concluded that FePc molecules underwent a pyrolysis process to get rid of all the H atoms during the heating process at 450°C in argon gas environment while the macrocyclic structure in FePc molecules remains in synthesized Fe-N_5-C/G catalyst. For Fe-N_5-C/G catalyst, the numbers of C-N bond and Fe-N bond remarkably increase while C-H bonds disappear compared with FePc(Fe-N_4) catalyst.

XPS analyses were conducted to investigate the chemical surroundings and elemental composition of synthesized Fe-N_5-C/G catalyst and FePc(Fe-N_4) catalyst. The survey spectrum shows distinctive peaks of element Fe, N, O and C, respectively (Fig.5a). The presence of the O1s peak is considered to be from the inevitable surface oxidation and pollutant. The results exhibit that element Fe, N and C are all the compositions of Fe-N_5-C/G catalyst and FePc(Fe-N_4) catalyst.

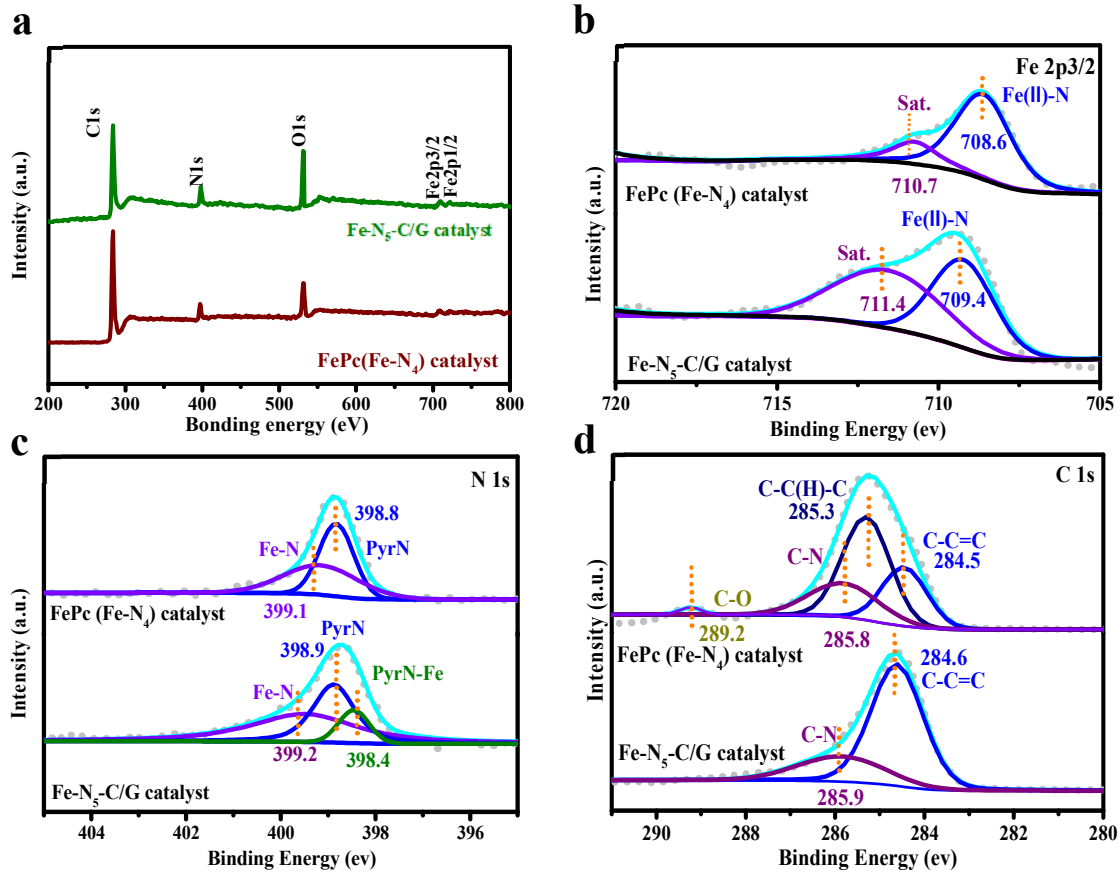

Figure 5. XPS spectra of Fe-N_5-C/G catalyst and FePc(Fe-N_4) catalyst. a) Survey spectrum, b) Fe 2p3/2 spectrum, c) N 1s, d) C 1s.

The Fe2p3/2 core level XPS spectrum of FePc(Fe-N_4) catalyst (Fig.5b) shows two peaks at 708.6 and 710.7 eV, corresponding to Fe(II) in Fe(II)-N bond and the satellite,[41-45] respectively. The peak corresponding to Fe(II) in Fe-N_5/G catalyst positively shifts to 709.4eV, indicating a decrease in the electron density around Fe(II) compared with that in FePc(Fe-N_4) catalyst. Combining the Raman analytic results that the macrocyclic structure still remains in Fe-N_5-C/G catalyst, the positive shift of the peak indicates that there is an additional interaction existing in Fe (II). The N 1s spectrum of FePc(Fe-N_4) catalyst (Fig.5c) can be deconvoluted into two peaks at 398.8 and 399.1eV, corresponding to the N atoms in pyridinic-N and Fe-N bond, respectively.[45]

The N 1s spectrum of Fe-N_5-C/G catalyst (Fig.5c) can be deconvoluted into three peaks at 398.4, 398.9 and 399.2eV, corresponding to three kinds of N atoms, respectively. Among the three kinds of N atoms, two kinds of the N atoms corresponding to the peaks at 398.9 and 399.2eV are the same as that in FePc(Fe-N_4) catalyst while the N atoms related with the peak at 398.4 eV are not exist in FePc(Fe-N_4) catalyst. The more negative binding energy for the new N atoms in Fe-N_5-C/G catalyst indicates that the electronic density around the new N atoms is higher than that in FePc(Fe-N_4) catalyst. Combining the decrease in the electronic density of Fe (II) in Fe-N_5-C/G catalyst, it can be concluded that some of the N atoms originaly acting as pyridinic-N in FePc(Fe-N_4) catalyst coordinate with Fe (II) in Fe-N_5-C/G catalyst to form new pyridinic-N-Fe bonds**.** In pyridinic-N-Fe bonds, the N atoms tend to obtain electrons and Fe (II) ions tend to lose electrons. Overall concidering Raman and FT-EXAFS analyses that all the macrocyclic structure in FePc(Fe-N_4) catalyst remains in synthesized Fe-N_5/G catalyst and the existence of the five-coordination structure as illustrated in Fig. 2c), it is believed that the coordination between pyridinic-N and Fe(II) takes place between Fe(II) and the pyridinic-N at the adjacent layer in Fe-N_5/G catalyst.

The C1s XPS spectrum of FePc(Fe-N_4) catalyst (Fig.5d) can be deconvoluted into four peaks at 284.5 eV, 285.3 eV, 285.8 eV and 289.2, which can be assigned to C-C=C, C-C(H)-C, C-N and C-O,[32] respectively. The C-O peak is considered to be from the inevitable surface oxidation and pollutant. For the C1s XPS spectrum of Fe-N_5-C/G catalyst, the peak corresponding to C-C(H)-C bonds in FePc(Fe-N_4) catalyst disappears while the other two peaks corresponding to C-C=C bonds and C-N bonds in FePc(Fe-N_4) catalyst remain, indicating that the bonds related with H atoms no longer exist in Fe-N_5-C/G catalyst and the H atoms in FePc molecules have been gotten rid of during the synthesizing process. In addition, the area size enclosed by the peak corresponding to C-C=C bonds in Fe-N_5-C/G catalyst becomes much

larger compared with that in PcFe(Fe-N_4) catalyst. It can be considered that the C atoms originally coordinating with H atoms in PcFe molecules coordinate again with C atoms to form C-C=C bond. The results demonstrate that a lot of new C-C=C bonds form in Fe-N_5-C/G catalyst.

2.8. ORR performances

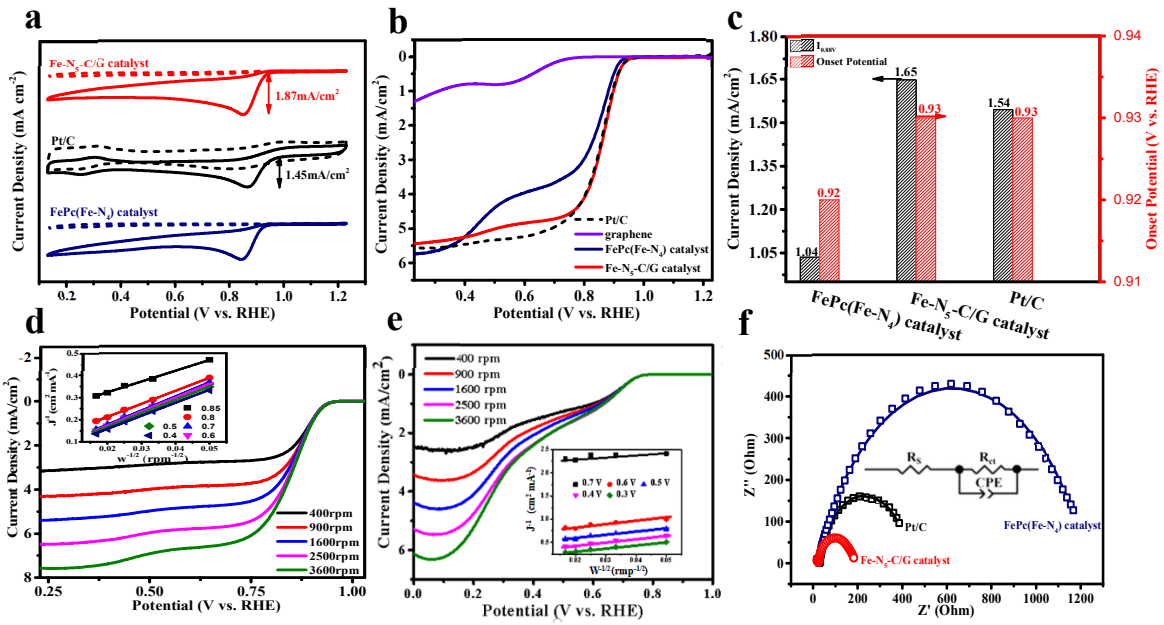

Figure 6. a) CVs curves of Fe-N_5-C/G catalyst, FePc(Fe-N_4) catalyst and commercial Pt/C catalyst in O_2-saturated (solid line) and N_2-saturated (dot line) electrolytes electrolytes, respectively; b) LSVs curves of Fe-N_5-C/G catalyst, FePc(Fe-N_4) catalyst and commercial Pt/C catalyst in O_2-saturated electrolytes, c) Comparison of the onset potential and current density (at 0.88V) for Fe-N_5-C/G catalyst, FePc(Fe-N_4) catalyst and commercial Pt/C catalyst. The data are from figure a), d) LSVs curves of Fe-N_5-C/G catalyst measured at different RDE rotating speed in O_2-saturated electrolytes, the inset is the K-L plots, e) LSVs curves of FePc(Fe-N_4) catalyst measured at different RDE rotating speed in O_2-saturated electrolytes, the inset is the K-L plots, f) EIS spectra of Fe-N_5-C/G catalyst, FePc(Fe-N_4) catalyst and commercial Pt/C catalyst measured at 0.91 V in O_2-saturated electrolytes. The inset is the equivalent circuit.

Fig. 6a) is the cyclic voltammetry (CV) curves of Fe-N_5-C/G catalyst, FePc(Fe-N_4) catalyst and commercial Pt/C catalyst measured in O_2- and N_2-saturated solution, respectively. In contrast to the virtually featureless CV curves measured in N_2-saturated solution, a notable cathodic peak appears in the CV curves of Fe-N_5-C/G catalyst (at 0.857), FePc(Fe-N_4) catalyst (at 0.845V) and Pt/C catalyst (at 0.865 V), in O_2-saturated solution, which can be attributed to the reduction of O_2.

The linear scanning voltammetry (LSV) was adopted to further investigate the ORR catalytic activity and the curves are shown in Fig. 6b). It can be found that the ORR current of synthesized graphene is extremely low. For clearly show the differences, the current densities at 0.88V (noted as $i_{0.88V}$) and the onset potentials derived from Fig. 6b) are plotted and shown in Fig. 6c). The onset potentials of Fe-N_5-C/G catalyst and Pt/C catalyst are the same (0.93V), which is more positive than that of FePc(Fe-N_4) catalyst (0.92V). The current density $i_{0.88V}$ of Fe-N_5-C/G catalyst (1.65 mA/cm^2) is 59% higher than that of FePc(Fe-N_4) catalyst (1.04 mA/cm^2), and even higher than that of commercial Pt/C catalyst (1.54 mA/cm^2). The results verify that Fe-N_5 active sites is more effective to catalyze ORR than Fe-N_4 active sites.

Fig. 6d) - e) are the LSV curves of Fe-N_5-C/G catalyst and FePc(Fe-N_4) catalyst measured at different rotating speeds and the insert is the K-L plots at different polarizing potentials, respectively. The current density goes up rapidly with the increase in the rotating speed. The electron transfer number (n) of the ORR for Fe-N_5-C/G catalyst and FePc(Fe-N_4) catalyst was calculated to be 4.01and 2.09, respectively, manifesting that an efficient four-electron transfer process takes place on Fe-N_5-C/G catalyst while a two-electron transfer process takes place on FePc(Fe-N_4) catalyst. The results indicate that the ORR proceeds through different path on Fe-N_4 active sites and Fe-N_5 active sites,

which reasonably explains why the electrocatalytic activity of Fe-N_5-C/G catalyst is superior to FePc(Fe-N_4) catalyst.

Electrochemical impedance spectroscopy (EIS) is a practical method to further understand the kinetics and interfacial properties of catalysts. Fig. 6f) gives the EIS plots of Fe-N_5-C/G catalyst, FePc(Fe-N_4) catalyst and commercial Pt/C catalyst, respectively. It can be seen that all the three AC impedance spectra show a semicircle. In order to better analyze the electrode process, an equivalent circuit (the inset in Fig. 6f) was used to fit the AC impedance spectrum. The fitting line is in good agreement with the measured data, indicating the rationality of the equivalent circuit. The equivalent circuit is composed of three components: a frequency-dependent constant phase element (CPE), a solution resistance (Rs) and a charge-transfer resistance (Rct). The simulated Rct value of Fe-N_5-C/G catalyst is 159Ω while that for FePc(Fe-N_4) catalyst and Pt/C catalyst are 1199 Ω and 408.2 Ω, respectively. The huge difference between Fe-N_5-C/G catalyst and FePc(Fe-N_4) catalyst in Rct values further confirms the ORR electrocatalytic activity of Fe-N_5 active sites is superior to that of FePc(Fe-N_4) active sites. The ranking order of the Rct values for the catalysts is 159Ω (Fe-N_5-C/G catalyst) < 408.2 Ω (Pt/C catalyst) < 1199 Ω (FePc(Fe-N_4) catalyst), which is consistent very well with that of the overpotentials calculated through DFT calculation (Fig. 1b).

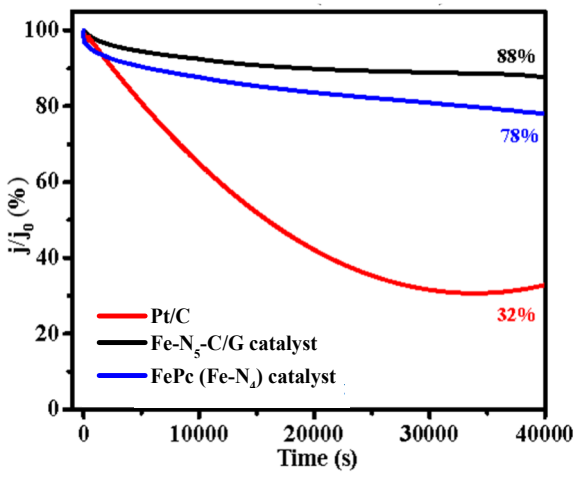

Figure 7. Chronoamperometric responses of Fe-N_5-C/G catalyst, commercial Pt/C catalyst and FePc(Fe-N_4) catalyst at potential 0.925V in O_2-saturated 0.1M KOH solution.

Chronoamperometric response curves were measured for Fe-N_5-C/G catalyst, FePc(Fe-N_4) catalyst and commercial Pt/C catalyst at potential 0.925V in O_2-saturated 0.1M KOH solution and shown in Fig. 7. For the ordinate J/J_0, J_0 represents the initial response current, J represents the response current after polarizing for a certain time. After chronoamperometric response at potential 0.925V for 40000s, the current reduces by 12%, 22% and 68% for Fe-N_5-C/G catalyst, FePc(Fe-N_4) catalyst and commercial Pt/C catalyst, respectively. The decrease of the current for FePc(Fe-N_4) catalyst is almost two times that for Fe-N_5-C/G catalyst. The decrease dergree of the response current can be used to estimate the discharge stability of catalysts. The results demonstrate that the discharge stability of Fe-N_5-C/G catalyst for ORR is much superior than FePc(Fe-N_4) catalyst. The discharge stability of commercial Pt/C catalyst is the worst.

The high discharge stability of Fe-N_5-C/G catalyst during ORR process can be considered to be due to the existence of the coordination structures among the layers, involving Fe(II)-N coordination structures and C-N coordination structures. The coordination structures strengthen the overall structure of the catalyst, thus prohibiting the degradation and dissolution of the active sites during polarizing process. Apart from the inherent structural stability of the catalysts, the structure stability of nonprecious metal catalysts for ORR has been frequently correlated with the amount of H_2O_2 species generated during ORR. It is possible that the four-electron transfer process of ORR is also an important contributing factor to the high discharge stability of Fe-N_5-C/G catalyst while the two-electron transfer process of ORR results in the poor

stability of FePc(Fe-N_4) catalyst. Therefore, 3D five-coordination structure Fe-N_5 active sites are more stable than 2D four-coordination structure Fe-N_4 active sites.

2.9. Proposed Formation mechanism for active site Fe-N_5

Electrochemical analyses demostrate that the enhanced electrocatalytic activity of synthesized Fe-N_5-C/G catalyst originates from the existence of great amount of Fe-N_5 active sites in its structure. SEM and HRTEM indicate that Fe-N_5-C/G catalyst possesses nano-fibre morphology and a layer-like crystal structure. The layer-like crystal structure is composed of great amounts of double-layer structural units joining together in a straight or curved way. XANES reveals that the Fe (II) in Fe-N_5-C/G catalyst is five-fold coordinated by five surrounding N atoms, in which four N atoms are located in the same plane and one N atom is located in the adjacent plane. Raman and XPS analyses demonstrate that FePc molecules underwent a dehydrogenation process during heating at 450°C in argon gas environment while the macrocyclic structure in FePc molecules remains in synthesized Fe-N_5-C/G catalyst. Compared with FePc(Fe-N_4) catalyst, the numbers of Fe-N bond, C-N bond and C-C bond increase in Fe-N_5-C/G catalyst.

Combining all the analyses, a formation mechanism about Fe-N_5-C/G catalyst are proposed and describe as follows (Fig. 8): during the heating process, FePc powders (the precursor) sublimate and get rid of the H atoms in its molecule to form unstable fragments in the space (Fig.8a). The unstable fragments in the space self-assemble mutually to form self-assembly units with double-layer structure. A five-coordination Fe-N_5 active site forms in the double-layer structured self-assembly units (Fig.8 b), in which a central Fe and its surrounded four N atoms are in the same fragment and there is a N atom located in the adjacent fragment. Then, the self-assembly units are driven by the flowing argon gas to another position at 70°C where the substrate is located in to

crystallize and form Fe-N_5-C/G catalyst. (Fig.8c). During the crystallizing process, some of the dehydrogenated C atoms in a self-assembly unit coordinate with the N atoms in the adjacent self-assembly unit located in different layer, and some of the dehydrogenated C atoms in two adjacent self-assembly units located in the same layers coordinate mutually. The existence of great amount of five-coordination Fe-N_5 active sites in the synthesied Fe-N_5-C/G catalyst promotes the ORR through an effective 4 electronic process. The interactions existing between the layers through C-N coordination and Fe(II)-N_5 coordination efficiently strengthen the structural stability of Fe-N_5-C/G catalyst. The formatin of great amount of C-C bonds in Fe-N_5-C/G catalyst makes the electronic transmission easier. These are the reasons for the high ORR performance of Fe-N_5-C/G catalyst.

3. Conclusions

DFT calculations indicate that the ORR electrocatalytic activity of Fe-N_5 active site embedded in carbon six-member rings is superior than that of Fe-N_4 active site. In order to experimentally verify the difference, iron phthalocyanine (FePc) powders was chosen as FePc(Fe-N_4) catalyst for its molecular structure involves a Fe-N_4 active site embeded in four carbon six-member rings, which is very close to the designed structural model with Fe-N_4 active site. Fe-N_5-C/G monatomic catalysts with Fe-N_5 active sites were successfully synthesized on the surface of monolayer graphene using FePc powders as the precursor. XANES, SEM, HRTEM, Raman and XPS analyses indicate that the synthesized Fe-N_5-C/G catalyst possesses nanofibre morphology and a layer-like crystal structure. Fe-N_5 active sites were formed in Fe-N_5-C/G catalyst through the five-fold coordination, in which a central Fe(II) ion and its surrounded four N atoms were located in the same layer and there is still a N atom located in the adjacent layer. The structure

of Fe-N_5-C/G catalyst is very close to the designed structural model with Fe-N_5 active site. The current density of synthesized Fe-N_5-C/G catalyst at potential 0.88Vvs RHE is 1.65 mA/cm^2, which is much higher than that of FePc(Fe-N_4) catalyst (1.04 mA/cm^2), and even higher than that of commercial Pt/C catalyst (1.54 mA/cm^2). All the texts were measured in an O2-saturated 0.1 M KOH solution at 25±1°C. An efficient four-electron transfer process takes place on Fe-N_5-C/G catalyst while a two-electron transfer process takes place on FePc(Fe-N_4) catalyst during ORR. The results are consistent very well with the DFT calculations, verifying the dependability and accuracy of DFT calculation.

A formation mechanism about Fe-N_5-C/G catalyst are proposed: during the heating process at 450°C, FePc powders (the precursor) sublimate and get rid of the H atoms in its molecule to form unstable fragments in the space. The unstable fragments in the space self-assemble mutually to form self-assembly units with double-layer structure. Then, great amounts of the self-assembly units are driven by the flowing argon gas to another position at 70°C where the substrate is located in to crystallize and form Fe-N_5-C/G catalyst. During the crystallizing process, some of the dehydrogenated C atoms in a self-assembly unit coordinate with the N atoms in the adjacent self-assembly unit located in different layer, and some of the dehydrogenated C atoms in two adjacent self-assembly units located in the same layers coordinate mutually.

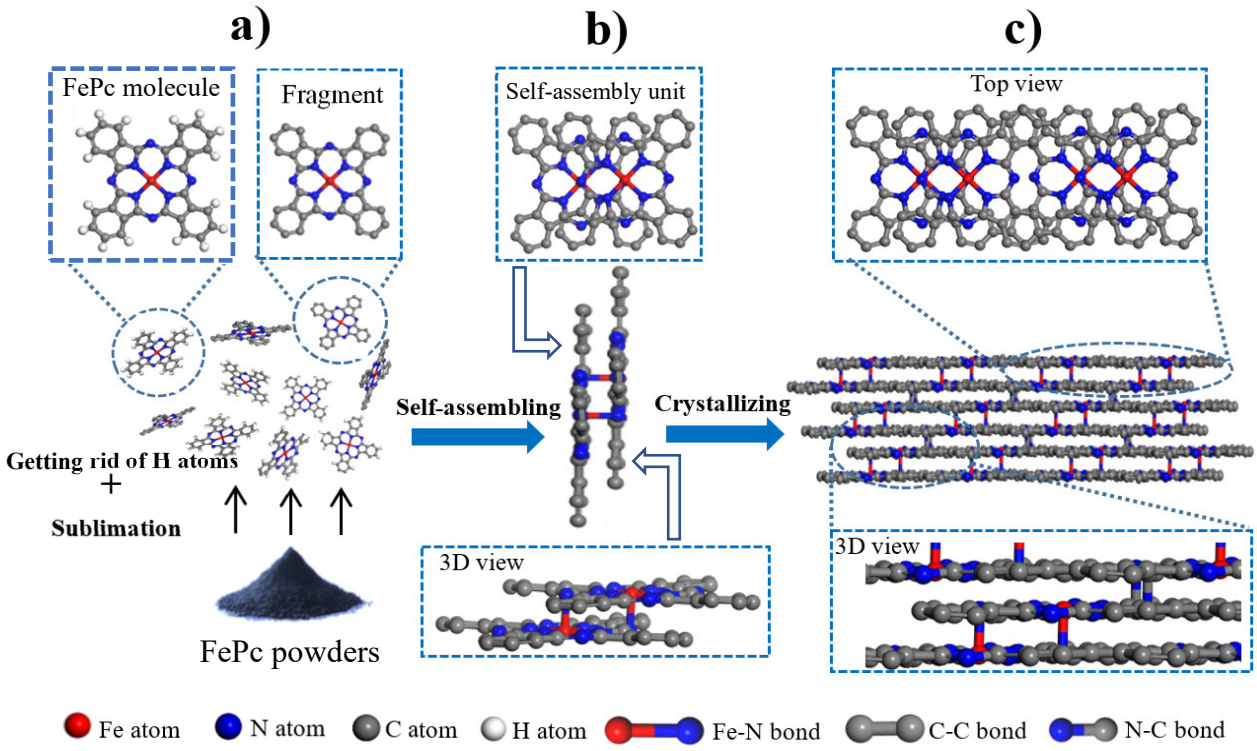

Figure 8. Schematic view of proposed forming process for Fe-N_5-C/G catalyst

Acknowledgements

The authors acknowledge the financial support of KEY LABORATORY OF METAL FUEL CELL OF SICHUAN PROVINCE.

Fan Liu and Ning Yan are the co-first authors.

Conflicts of interest

The authors declare no conflict of interest.

References

[1] X. Wu, F. Chen, N. Zhang, A. Qaseem and R. L. Johnston, Small, 2017, 13.

[2] G. Saianand, A. I. Gopalan, J. C. Lee, C. I. Sathish, K. Gopalakrishnan, G. E. Unni, D. Shanbhag, V. Dasireddy, J. Yi, S. Xi, A. H. Al-Muhtaseb and A. Vinu, Small, 2020, 16, e1903937.

[3] H. Yoon, S. Lee, S. Oh, H. Park, S. Choi and M. Oh, Small, 2019, 15, e1805232.

[4] J. Suntivich, H. A. Gasteiger, N. Yabuuchi, H. Nakanishi, J. B. Goodenough and Y. Shao-Horn, Nature chemistry, 2011, 3, 546-550.

[5] M. K. Debe, Nature, 2012, 486, 43-51.

[6] B. Kang, X. Jin, S. M. Oh, S. B. Patil, M. G. Kim, S. H. Kim and S.-J. Hwang, Applied Catalysis B: Environmental, 2018, 236, 107-116.

[7] C. Wei, Z. Feng, G. G. Scherer, J. Barber, Y. Shao-Horn and Z. J. Xu, Adv Mater, 2017, 29.

[8] Y. F. Sun, Y. Q. Zhang, J. Chen, J. H. Li, Y. T. Zhu, Y. M. Zeng, B. S. Amirkhiz, J. Li, B. Hua and J. L. Luo, Nano Lett, 2016, 16, 5303-5309.

[9] M. B. Stevens, C. D. M. Trang, L. J. Enman, J. Deng and S. W. Boettcher, J Am Chem Soc, 2017, 139, 11361-11364.

[10] Q. Li, R. Cao, J. Cho and G. Wu, Advanced Energy Materials, 2014, 4.

[11] L. Zhao, X.-L. Sui, J.-Z. Li, J.-J. Zhang, L.-M. Zhang, G.-S. Huang and Z.-B. Wang, Applied Catalysis B: Environmental, 2018, 231, 224-233.

[12] H. Tabassum, R. Zou, A. Mahmood, Z. Liang, Q. Wang, H. Zhang, S. Gao, C. Qu, W. Guo and S. Guo, Adv Mater, 2018, 30.

[13] Y.-Q. Zhang, M. Li, B. Hua, Y. Wang, Y.-F. Sun and J.-L. Luo, Applied Catalysis B: Environmental, 2018, 236, 413-419.

[14] Y.-J. Ko, K. Choi, B. Yang, W. H. Lee, J.-Y. Kim, J.-W. Choi, K. H. Chae, J. H. Lee, Y. J. Hwang, B. K. Min, H.-S. Oh and W.-S. Lee, Journal of Materials Chemistry A, 2020, 8, 9859-9870.

[15] M. K. Jana and C. N. Rao, Philos Trans A Math Phys Eng Sci, 2016, 374.

[16] J. Wu, M. T. Rodrigues, R. Vajtai and P. M. Ajayan, Adv Mater, 2016, 28, 6239-6246.

[17] L. Zhao, Y. Zhang, L. B. Huang, X. Z. Liu, Q. H. Zhang, C. He, Z. Y. Wu, L. J. Zhang, J. Wu, W. Yang, L. Gu, J. S. Hu and L. J. Wan, Nat Commun, 2019, 10, 1278.

[18] Y.-C. Wang, Y.-J. Lai, L. Song, Z.-Y. Zhou, J.-G. Liu, Q. Wang, X.-D. Yang, C. Chen, W. Shi, Y.-P. Zheng, M. Rauf and S.-G. Sun, Angewandte Chemie International Edition, 2015, 54, 9907-9910.

[19] J. Shui, C. Chen, L. Grabstanowicz, D. Zhao and D. J. Liu, Proc Natl Acad Sci U S A, 2015, 112, 10629-10634.

[20] Y. J. Sa, D. J. Seo, J. Woo, J. T. Lim, J. Y. Cheon, S. Y. Yang, J. M. Lee, D. Kang, T. J. Shin, H. S. Shin, H. Y. Jeong, C. S. Kim, M. G. Kim, T. Y. Kim and S. H. Joo, J Am Chem Soc, 2016, 138, 15046-15056.

[21] H. Zhao, C. Sun, Z. Jin, D.-W. Wang, X. Yan, Z. Chen, G. Zhu and X. Yao, Journal of Materials Chemistry A, 2015, 3, 11736-11739.

[22] Z. Liu, Z. Zhao, Y. Wang, S. Dou, D. Yan, D. Liu, Z. Xia and S. Wang, Adv Mater, 2017, 29.

[23] H. Zhang, S. Hwang, M. Wang, Z. Feng, S. Karakalos, L. Luo, Z. Qiao, X. Xie, C. Wang, D. Su, Y. Shao and G. Wu, J Am Chem Soc, 2017, 139, 14143-14149.

[24] L. Lin, Q. Zhu and A. W. Xu, J Am Chem Soc, 2014, 136, 11027-11033.

[25] W. J. Jiang, L. Gu, L. Li, Y. Zhang, X. Zhang, L. J. Zhang, J. Q. Wang, J. S. Hu, Z. Wei and L. J. Wan, J Am Chem Soc, 2016, 138, 3570-3578.

[26] C. Zhu, S. Fu, J. Song, Q. Shi, D. Su, M. H. Engelhard, X. Li, D. Xiao, D. Li, L. Estevez, D. Du and Y. Lin, Small, 2017, 13.

[27] Q. Wang, Z. Y. Zhou, Y. J. Lai, Y. You, J. G. Liu, X. L. Wu, E. Terefe, C. Chen, L. Song, M. Rauf, N. Tian and S. G. Sun, J Am Chem Soc, 2014, 136, 10882-10885.

[28] X. Zhang, R. Liu, Y. Zang, G. Liu, G. Wang, Y. Zhang, H. Zhang and H. Zhao, Chemical Communications, 2016, 52, 5946-5949.

[29] P. Subramanian, R. Mohan and A. Schechter, ChemCatChem, 2017, 9, 1969-1978.

[30] G. Wu, K. L. More, P. Xu, H. L. Wang, M. Ferrandon, A. J. Kropf, D. J. Myers, S. Ma, C. M. Johnston and P. Zelenay, Chem Commun (Camb), 2013, 49, 3291-3293.

[31] W. Liang, J. Chen, Y. Liu and S. Chen, ACS Catalysis, 2014, 4, 4170-4177.

[32] G. Zhu, F. Liu, Y. Wang, Z. Wei and W. Wang, Phys Chem Chem Phys, 2019, 21, 12826-12836.

[33] X. S. Li, W. W. Cai, J. H. An, S. Kim, J. Nah, D. X. Yang, R. Piner, A. Velamakanni, I. Jung, E. Tutuc, S. K. Banerjee, L. Colombo and R. S. Ruoff, Science, 2009, 324, 1312-1314.

[34] Y. Garsany, O. A. Baturina, K. E. Swider-Lyons and S. S. Kocha, Anal. Chem., 2010, 82, 6321-6328.

[35] M. Sun, D. Davenport, H. Liu, J. Qu, M. Elimelech and J. Li, Journal of Materials Chemistry A, 2018, 6, 2527-2539.

[36] B. Mecheri, V. C. A. Ficca, M. A. Costa de Oliveira, A. D'Epifanio, E. Placidi, F. Arciprete and S. Licoccia, Applied Catalysis B: Environmental, 2018, 237, 699-707.

[37] J. Guo, X. Yan, Q. Liu, Q. Li, X. Xu, L. Kang, Z. Cao, G. Chai, J. Chen, Y. Wang and J. Yao, Nano Energy, 2018, 46, 347-355.

[38] S. Kattel, P. Atanassov and B. Kiefer, Phys Chem Chem Phys, 2014, 16, 13800-13806.

[39] F. Liu, G. Zhu, D. Yang, D. Jia, F. Jin and W. Wang, RSC Advances, 2019, 9, 22656-22667.

[40] A. N. Filippin, V. c. López-Flores, T. C. Rojas, Z. Saghi, V. J. Rico, J. R. Sanchez-Valencia, J. P. Espinós, A. Zitolo, M. Viret, P. A. Midgley, A. Barranco and A. Borras, Chemistry of Materials, 2018, 30, 879-887.

[41] C. Jennings, R. Aroca , A. Hor and R. 0. Loutfy, Journal of Raman Spectroscopy, 1984, 15(1):34-37.

[42] Q. Zhao, M. Hou, S. Jiang, S. Wang, J. Ai, L. Zheng and Z. Shao, RSC Advances, 2016, 6, 80024-80028.

[43] K. Artyushkova, A. Serov, S. Rojas-Carbonell and P. Atanassov, The Journal of Physical Chemistry C, 2015, 119, 25917-25928.

[44] W. Cai, J. Zhou, G. Li, K. Zhang, X. Liu, C. Wang, H. Zhou, Y. Zhu and Y. Qian, ACS Appl Mater Interfaces, 2016, 8, 27679-27687.

[45] Y. Li, W. Zhou, H. Wang, L. Xie, Y. Liang, F. Wei, J. C. Idrobo, S. J. Pennycook and H. Dai, Nat Nanotechnol, 2012, 7, 394-400.